

Jan Valášek; Petr Sváček; Jaromír Horáček

On finite element approximation of flow induced vibration of elastic structure

In: Jan Chleboun and Pavel Kůs and Petr Příkryl and Karel Segeth and Jakub Šístek and Tomáš Vejchodský (eds.): Programs and Algorithms of Numerical Mathematics, Proceedings of Seminar. Janov nad Nisou, June 19-24, 2016. Institute of Mathematics CAS, Prague, 2017. pp. 144–153.

Persistent URL: <http://dml.cz/dmlcz/703008>

Terms of use:

© Institute of Mathematics CAS, 2017

Institute of Mathematics of the Czech Academy of Sciences provides access to digitized documents strictly for personal use. Each copy of any part of this document must contain these *Terms of use*.



This document has been digitized, optimized for electronic delivery and stamped with digital signature within the project *DML-CZ: The Czech Digital Mathematics Library*
<http://dml.cz>

ON FINITE ELEMENT APPROXIMATION OF FLOW INDUCED VIBRATION OF ELASTIC STRUCTURE

Jan Valášek¹, Petr Sváček¹, Jaromír Horáček²

¹ Faculty of Mechanical Engineering, CTU in Prague
Karlovo nám. 13, Praha 2, 121 35, Czech Republic
valasek.jan@volny.cz, petr.svacek@fs.cvut.cz

² Institute of Thermomechanics, The Czech Academy of Sciences
Dolejškova 5, 182 00 Praha 8, Czech Republic
jaromirh@it.cas.cz

Abstract: In this paper the fluid-structure interaction problem is studied on a simplified model of the human vocal fold. The problem is mathematically described and the arbitrary Lagrangian-Eulerian method is applied in order to treat the time dependent computational domain. The viscous incompressible fluid flow and linear elasticity models are considered. The fluid flow and the motion of elastic body is approximated with the aid of finite element method. An attention is paid to the applied stabilization technique. The whole algorithm is implemented in an in-house developed solver. Numerical results are presented and the influence of different inlet boundary conditions is discussed.

Keywords: stabilized finite element method, 2D Navier-Stokes equations, vocal folds, aeroelasticity

MSC: 65M60, 35Q30, 76D05

1. Introduction

The flow induced vibration of elastic structure or more generally fluid-structure interaction problems (FSI) are important in many technical applications, see e.g. [3]. This contribution focuses on the simulation of human vocal folds vibration, see e.g. [5]. There are many numerical methods concerned with the solution of the fluid-structure interaction and also many approaches how to deal with the coupled problem. Basically these can be characterized as either the monolithic or partitioned scheme, see for example [7]. Monolithic solvers are usually more robust, but more computer time consuming. The partitioned scheme decouples the solution of both subproblems, but on the other hand it often requires subiterations.

This paper focuses on the application of the partitioned scheme for finite element method (FEM). To avoid possible instabilities of FEM due to high Reynolds

number flows the streamline upwind/Petrov-Galerkin (SUPG) method, pressure-stabilization/Petrov-Galerkin (PSPG) method together with ‘div-div’ stabilization are applied.

The structure of the paper is as follows. First the mathematical model consisting of the Navier-Stokes and linear elasticity equations is presented and the arbitrary Lagrangian-Eulerian method (ALE) is used. Further the flow problem is discretized in space by the stabilized finite element method. The numerical results of several test cases are shown.

2. Mathematical model

For the sake of simplicity the FSI problem is solved in 2D. The geometry of the problem topology is shown in Figure 1. The elastic structure (the vocal fold) is represented by the domain Ω^s . It is not necessary to distinguish between the shape at an arbitrary time t and the reference shape of the domain because of the adopted Lagrange approach for the deformation description.

The domain Ω_{ref}^f denotes the reference fluid domain, e.g. the domain at the time instant $t = 0$ with the common interface $\Gamma_{W_{ref}} = \Gamma_{W_0}$ between the fluid and structure domains. The fluid motion is solved with the ALE method, which enables the change of the reference domain Ω_{ref}^f to the domain Ω_t^f at any time instant t .

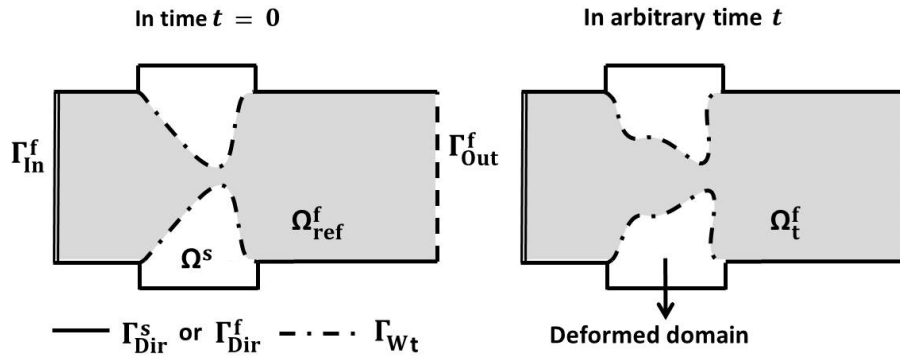


Figure 1: Geometry of vocal folds model with boundaries marked before (left) and after (right) deformation.

Elastic body. The deformation of the elastic body Ω_{ref}^s depends on establishing of dynamic equilibrium between the inertia forces and the applied surface and volume forces. This equilibrium is described by the partial differential equation, see e.g. [2]

$$\rho^s \frac{\partial^2 u_i}{\partial t^2} - \frac{\partial \tau_{ij}^s}{\partial x_j} = f_i^s \quad \text{in } \Omega^s \times (0, T), \quad (1)$$

where $\mathbf{u}(X, t) = (u_1, u_2)$ denotes the displacement vector, f_i^s is the component of volume force, ρ^s is the structure density and τ_{ij} are the components of the Cauchy

stress tensor. These components are expressed by the generalized Hooke's law. Assuming the isotropic material and small displacements the components of the stress tensor $\boldsymbol{\tau}^s = (\tau_{ij}^s)$ are given by

$$\tau_{ij}^s = \lambda^s (\operatorname{div} \mathbf{u}) \delta_{ij} + 2\mu^s e_{ij}^s(\mathbf{u}), \quad (2)$$

where δ_{ij} is Kronecker's delta, $e_{jk}^s(\mathbf{u}) = \frac{1}{2} \left(\frac{\partial u_j}{\partial x_k} + \frac{\partial u_k}{\partial x_j} \right)$ is the strain tensor, and λ^s, μ^s are Lamé's constants related to the Young modulus of elasticity and Poisson's ratio. The partial differential equation (1) is enclosed with the following initial and boundary conditions

$$\begin{aligned} \text{a)} \quad & \mathbf{u}(X, 0) = \mathbf{u}_0(X), \quad \text{for } X \in \Omega^s, \\ \text{b)} \quad & \frac{\partial \mathbf{u}}{\partial t}(X, 0) = \mathbf{u}_1(X) \quad \text{for } X \in \Omega^s, \\ \text{c)} \quad & \mathbf{u}(X, t) = \mathbf{u}_{\text{Dir}}(X, t) \quad \text{for } X \in \Gamma_{\text{Dir}}^s, \quad t \in (0, T), \\ \text{d)} \quad & \tau_{ij}^s(X, t) n_j^s(X) = q_i^s(X, t), \quad \text{for } X \in \Gamma_{\text{Wref}}^s, \quad t \in (0, T), \end{aligned} \quad (3)$$

where the $\Gamma_{\text{Wref}}^s, \Gamma_{\text{Dir}}^s$ are mutually disjoint parts of the boundary $\partial\Omega = \Gamma_{\text{Wref}}^s \cup \Gamma_{\text{Dir}}^s$ (see Figure 1) and $n_j^s(X)$ are components of the unit outer normal to Γ_{Wref}^s .

ALE method. The ALE method uses a diffeomorphism A_t of the reference (undeformed) domain Ω_{ref}^f onto the time-dependent domain Ω_t^f at any time instant $t \in (0, T)$. This mapping A_t is also required to satisfy

$$\frac{\partial A_t}{\partial t} \in C(\Omega_{\text{ref}}^f), \quad A_t(\partial\Omega_{\text{ref}}^f) = \partial\Omega_t^f, \quad t \in (0, T). \quad (4)$$

The ALE domain velocity is then defined by

$$\mathbf{w}_D(x, t) = \frac{\partial}{\partial t} A_t(X), \quad t \in (0, T), \quad x = A_t(X) \in \Omega_t^f. \quad (5)$$

Afterwards ALE derivative is introduced as the time derivative with respect to a fixed point $X \in \Omega_{\text{ref}}^f$. The ALE derivative satisfies

$$\frac{D^A}{Dt} f(x, t) = \frac{df(A_t(X), t)}{dt} = \frac{\partial f}{\partial t}(x, t) + \mathbf{w}_D(x, t) \cdot \nabla f(x, t). \quad (6)$$

For more details see the article [9]. The practical construction of ALE mapping is described in [5] or [10].

Fluid motion. The fluid is assumed to be viscous and incompressible in the time dependent domain Ω_t^f . Its motion is modelled by the Navier-Stokes equations in the ALE form

$$\frac{D^A \mathbf{v}}{Dt} + ((\mathbf{v} - \mathbf{w}_D) \cdot \nabla) \mathbf{v} - \nu^f \Delta \mathbf{v} + \nabla p = \mathbf{0}, \quad \operatorname{div} \mathbf{v} = 0 \quad \text{in } \Omega_t^f, \quad (7)$$

where $\mathbf{v}(x, t)$ denotes the fluid velocity, p is the kinematic pressure and ν^f is the kinematic fluid viscosity, see [5].

The problem (7) is equipped with an initial and the following boundary conditions

$$\begin{aligned} \text{a)} \quad & \mathbf{v}(x, t) = \mathbf{w}_D(x, t) && \text{for } x \in \Gamma_{\text{Dir}}^f \cup \Gamma_{\text{W}_t}, t \in (0, T), \\ \text{b)} \quad & \mathbf{v}(x, t) = \mathbf{v}_{\text{Dir}}(x, t) && \text{for } x \in \Gamma_{\text{In}}^f, t \in (0, T), \\ \text{c)} \quad & p(x, t)\mathbf{n}^f - \nu^f \frac{\partial \mathbf{v}}{\partial \mathbf{n}^f}(x, t) = -\frac{1}{2}\mathbf{v}(\mathbf{v} \cdot \mathbf{n}^f)^- && \text{for } x \in \Gamma_{\text{Out}}^f, t \in (0, T), \end{aligned} \quad (8)$$

where \mathbf{n}^f is unit outer normal to boundary $\partial\Omega_t^f$. The last condition (8 c) is the modified do-nothing boundary condition according to [1], which suppresses possible backward inlet through the outlet boundary.

Coupling. The solutions of problems (1) and (7) depend on each other via the boundary conditions on the common interface. Moreover, the location of the interface Γ_{W_t} at time t is not a priori known and is dependent on the establishing force equilibrium between the aerodynamic and the elastic forces. It is implicitly given by the deformation \mathbf{u} as

$$\Gamma_{\text{W}_t} = \{x \in \mathbb{R}^2 \mid x = X + \mathbf{u}(X, t), X \in \Gamma_{\text{W}_{\text{ref}}}\}. \quad (9)$$

First the so called dynamic boundary condition expressing effect of aerodynamic force $\mathbf{q}^s = (q_1^s, q_2^s)$ is prescribed at the interface for the structure, where

$$q_i^s(X, t) = - \sum_{j=1}^2 \rho^f (-p\delta_{ij} + \nu^f (\frac{\partial \mathbf{v}_i}{\partial x_j} + \frac{\partial \mathbf{v}_j}{\partial x_i})) n_j^f \Big|_{x=X+\mathbf{u}(X,t)}. \quad (10)$$

Further, the coupling of the problem is characterized by the so called kinematic boundary condition (8a), where the domain velocity \mathbf{w}_D is equal to the structure velocity at the interface Γ_{W_t} . In order to solve the problem, the strong coupling algorithm is implemented, see e.g. [5].

3. Discretization

Both parts of the FSI problem were discretized in space by the finite element method. For the time discretization the equidistant time step $\Delta t = \frac{T}{N}$, $N \gg 1$ was used. The partition of the time interval is then given by $t_n = n\Delta t$. The functions $\mathbf{u}, \mathbf{v}, p$ are approximated at time instant t_n by $\mathbf{u}^n, \mathbf{v}^n, p^n$.

Elastic body. First, equation (1) is reformulated in a weak sense, the generalized Hooke's law (2) and the Green theorem is applied, which leads to

$$\left(\rho^s \frac{\partial^2 u_j}{\partial t^2}, \varphi_j \right)_{\Omega^s} + (\lambda^s (\text{div } \mathbf{u}) \delta_{ij} + 2\mu^s e_{ij}^s(\mathbf{u}), e_{ij}^s(\boldsymbol{\varphi}))_{\Omega^s} = (f_j^s, \varphi_j)_{\Omega^s} + (q_j^s, \varphi_j)_{\Gamma_{\text{Neu}}^s}. \quad (11)$$

This equation needs to be satisfied for all $\boldsymbol{\varphi} = (\varphi_1, \varphi_2) \in V \times V$, where $V = \{\phi \in H^1(\Omega^s) | \phi = 0 \text{ on } \Gamma_{\text{Dir}}^s\}$ and $H^1(\Omega)$ is the Sobolev's space. The notation $(\cdot, \cdot)_M$ denotes scalar product in the space $L^2(M)$. The numerical solution \mathbf{u}_h is now sought in the finite dimensional FE space, i.e. it can be expressed as the linear combination of basis functions $\mathbf{u}_h(x, t) = \sum_{i=1}^{N_h} \alpha_i(t) \boldsymbol{\varphi}_i(x)$, where the coefficients $\boldsymbol{\alpha}(t) = (\alpha_i(t))$ are unknowns. Then fulfilment of equation (11) leads to the system of ordinary differential equations of the second order

$$\mathbb{M}\ddot{\boldsymbol{\alpha}}(t) + \mathbb{C}\dot{\boldsymbol{\alpha}}(t) + \mathbb{K}\boldsymbol{\alpha}(t) = \mathbf{b}(t), \quad (12)$$

where the matrix \mathbb{C} was added as a model of the proportional structural damping, see e.g. [5]. The vector $\mathbf{b}(t)$ has components $b_j(t) = (\mathbf{f}^s, \boldsymbol{\varphi}_j)_{\Omega^s} + (\mathbf{q}^s, \boldsymbol{\varphi}_j)_{\Gamma_{\text{Neu}}^s}$ and the elements of matrices $\mathbb{M} = (m_{ij}), \mathbb{K} = (k_{ij})$ are given by

$$m_{ij} = \left(\rho^s \frac{\partial^2 \boldsymbol{\varphi}_i}{\partial t^2}, \boldsymbol{\varphi}_j \right)_{\Omega^s}, \quad k_{ij} = \left(\lambda^s (\text{div } \boldsymbol{\varphi}_i) \delta_{rl} + 2\mu^s e_{rl}^s(\boldsymbol{\varphi}_i), e_{rl}^s(\boldsymbol{\varphi}_j) \right)_{\Omega^s}. \quad (13)$$

The proportional damping matrix is chosen as $\mathbb{C} = \epsilon_1 \mathbb{M} + \epsilon_2 \mathbb{K}$ with appropriate choice of parameters ϵ_1, ϵ_2 . This system is numerically approximated by the Newmark method, see e.g. [5].

Fluid motion. Equation (7) is first discretized in time by the backward differentiation formula of the second order (BDF2), see [10]. Furthermore, the nonlinear convective term is linearized using the value from the previous time step, $(\mathbf{v} \cdot \nabla) \mathbf{v}|_{t_{n+1}} \approx (\mathbf{v}^n \cdot \nabla) \mathbf{v}^{n+1}$. Afterwards the weak formulation is derived in the standard way, where on the outflow part of the boundary Γ_{Out}^f one extra application of Green theorem to the convective term according to [1] is performed. The functional spaces $\mathbf{X} = X \times X$, $X = H^1(\Omega^f)$ and $M = L^2(\Omega^f)$ are introduced. Then the solution of problem $V = (\mathbf{v}, p) = (\mathbf{v}^{n+1}, p^{n+1})$ is sought in the space $\mathbf{X} \times M$ such that \mathbf{v} fulfills conditions (8 a) b)) and moreover

$$a(V, \Phi) = f(\Phi) \quad \text{for all } \Phi = (\boldsymbol{\varphi}, q) \in \mathbf{W} \times L^2(\Omega^f), \quad (14)$$

where $\mathbf{W} = W \times W$, $W = \{\phi \in X | \phi = 0 \text{ on } \Gamma_{\text{Dir}}^f \cup \Gamma_{\text{In}}^f \cup \Gamma_{\text{Wt}}^f\}$. The bilinear form $a(\cdot, \cdot)$ and functional $f(\cdot)$ are defined as

$$\begin{aligned} a(V, \Phi) &= \left(\frac{3\mathbf{v}}{2\Delta t}, \boldsymbol{\varphi} \right)_{\Omega^f} + \frac{1}{2} ((\bar{\mathbf{v}}^n - 2\mathbf{w}_D) \cdot \nabla) \mathbf{v}, \boldsymbol{\varphi} \Big|_{\Omega^f} - \frac{1}{2} ((\bar{\mathbf{v}}^n \cdot \nabla) \boldsymbol{\varphi}, \mathbf{v}) \Big|_{\Omega^f} + \\ &+ \frac{1}{2} ((\bar{\mathbf{v}}^n \cdot \mathbf{n}^f)^+ \mathbf{v}, \boldsymbol{\varphi}) \Big|_{\Gamma_{\text{Out}}^f} + \nu^f (\nabla \mathbf{v}, \nabla \boldsymbol{\varphi}) \Big|_{\Omega^f} - (p, \text{div } \boldsymbol{\varphi}) \Big|_{\Omega^f} + (q, \text{div } \mathbf{v}) \Big|_{\Omega^f}, \quad (15) \\ f(\Phi) &= \left(\frac{4\bar{\mathbf{v}}^n - \bar{\mathbf{v}}^{n-1}}{2\Delta t}, \boldsymbol{\varphi} \right)_{\Omega^f}, \end{aligned}$$

where for a given time step t_{n+1} we set $\bar{\mathbf{v}}^i(x) = \mathbf{v}^i(A_{t_i}(A_{t_{n+1}}^{-1}(x)))$.

Stabilization of FEM. The instability arises primarily from unresolved high velocity gradients regions, which can be characterized by high values of local Reynold number Re_K . In order to overcome this phenomenon the streamline-upwind/Petrov-Galerkin method (SUPG) and pressure-stabilization method (PSPG) together with ‘div-div stabilization’ were applied, see [6]. The fully stabilized scheme is introduced with the additional terms added to equation (14) with shortened notation $\zeta := ((\bar{\mathbf{v}}^n - \mathbf{w}_D) \cdot \nabla)\boldsymbol{\varphi} + \nabla q$

$$\begin{aligned} \mathcal{L}(V, \Phi) &= \sum_{K \in \mathcal{T}_h} \delta_K \left(\frac{3\mathbf{v}}{2\Delta t} + ((\bar{\mathbf{v}}^n - \mathbf{w}_D) \cdot \nabla)\mathbf{v} + \nabla p - \nu \Delta \mathbf{v}, \zeta \right)_K, \\ \mathcal{F}(\Phi) &= \sum_{K \in \mathcal{T}_h} \delta_K \left(\frac{4\bar{\mathbf{v}}^n - \bar{\mathbf{v}}^{n-1}}{2\Delta t}, \zeta \right)_K, \quad \mathcal{P}(V, \Phi) = \sum_{K \in \mathcal{T}_h} \tau_K (\nabla \cdot \mathbf{v}, \nabla \cdot \boldsymbol{\varphi})_K, \end{aligned} \quad (16)$$

where parameters δ_K and τ_K are locally defined using local element length h_K as

$$\delta_K = \frac{h_K^2}{\tau_K}, \quad \tau_K = \nu \left(1 + Re^K + \frac{h_K^2}{\nu \Delta t} \right), \quad Re^K = \frac{h_K \| \bar{\mathbf{v}}^n - \mathbf{w}_D \|_K}{2\nu}. \quad (17)$$

The stabilized problem now reads: find $V = (\mathbf{v}, p) \in \mathbf{X} \times M$ such that \mathbf{v} fulfills conditions (8a)b) and

$$a(V, \Phi) + \mathcal{L}(V, \Phi) + \mathcal{P}(V, \Phi) = f(\Phi) + \mathcal{F}(\Phi), \quad (18)$$

for all $\Phi = (\boldsymbol{\varphi}, q) \in \mathbf{W} \times L^2(\Omega^f)$. The numerical simulations were done using LBB stable P1-bubble/P1 elements. The solution of system (18) was performed by the mathematical library UMFPACK, see [4].

4. Numerical simulations

Numerical tests were performed on computational domain with vocal fold model M5 described in [8]. The height of the vocal fold was set to 6 mm.

Flow solver. First, the fluid flow through the fixed computational domain without interaction was computed. The inlet velocity was set to fully developed flow with maximum 1 m/s. The viscosity was set to $\nu^f = 1.47 \cdot 10^{-5} \text{ m}^2/\text{s}$ and the time step $\Delta t = 10^{-4} \text{ s}$ was chosen. Figure 2 shows a distribution of the flow velocity magnitude and pressure and illustrates the typical jet and vortex structures. Figure 3 shows the pressure difference between the inlet and the outlet computed both with (p_stab) and without stabilization (p_unstab). For this computation it was possible to use also the unstabilized FEM, the results are very similar.

FSI test. Subsequently, the coupled fluid-structure interaction problem in the same domain was solved. The vocal fold consists of two layers: The thin layer around the interface represents epithelium with Young modulus of elasticity and Poisson’s

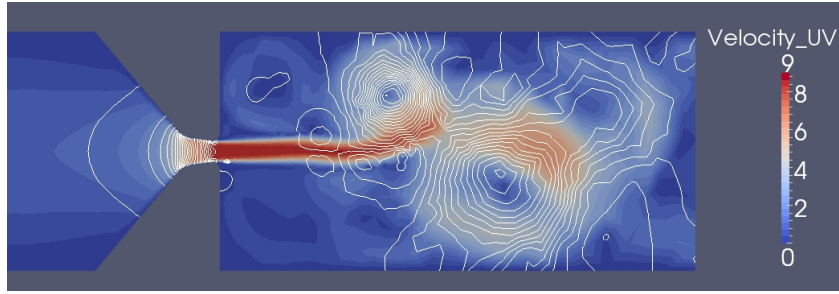


Figure 2: Flow field velocity together with pressure isolines are shown at the time instant $t = 0.3105$ s for the case of the unstabilized FEM computation.

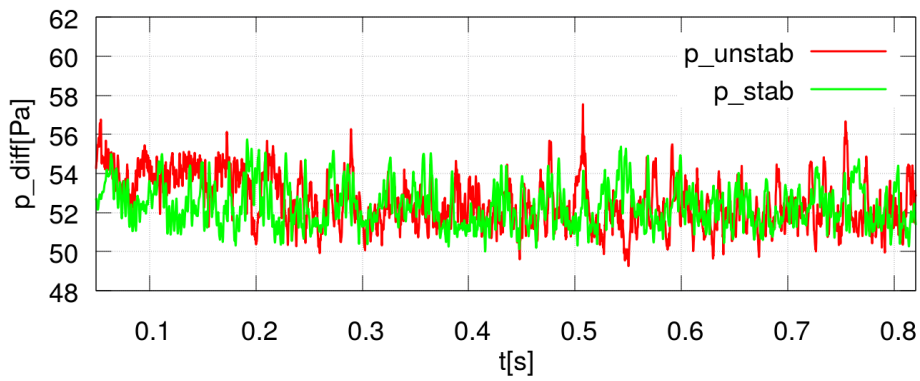


Figure 3: Pressure difference between the mean value on the inlet and the outlet.

ratio $E^s = 100$ kPa and $\sigma = 0.4$, respectively. The rest of the vocal fold (muscle) is modelled with $E^s = 12$ kPa, $\sigma = 0.4$. The densities were set as $\rho^s = 1000$ kg/m³, $\rho^f = 1.185$ kg/m³ and damping parameters as $\epsilon_1 = 5.0$ s⁻¹, $\epsilon_2 = 2.0 \cdot 10^{-5}$ s. The eigenfrequencies and the eigenmodes were determined by the modal analysis. The first two are shown in Figure 4. They are the most important because the first mode represents motion dominantly in x -direction, whereas the second in the y -direction. The higher eigenfrequencies have a more complex shape of eigenmodes.

The same problem was solved either with the prescribed inlet velocity (parabolic profile with maximum 3 m/s - BC_velocity) or with the prescribed correspondent pressure difference (272.55 Pa - BC_pressure). The interaction between elastic body and fluid flow was enabled after 0.1 s of computation, when the flow field was already fully developed. The numerically simulated displacements of one chosen node at the top of the bottom vocal fold are plotted in Figures 5 and 6 on the left and the Fourier transforms of the time signal are shown on the right.

After a transient part of the simulation, that corresponds to a sudden loading of the vocal folds by aerodynamic forces at the start of the interaction, the vocal folds vibrate with similar amplitudes in both cases around a new equilibrium point. The Fourier transform indicates the excitation of the first two eigenmodes. The first

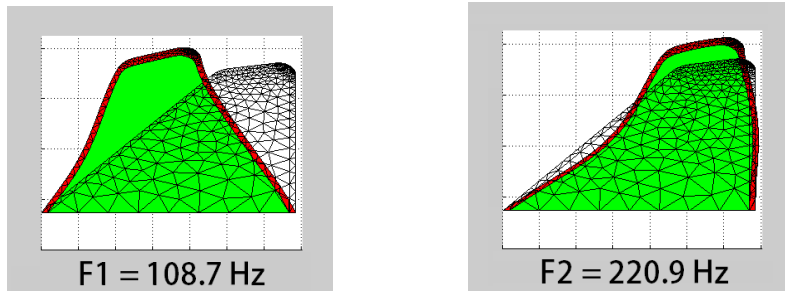


Figure 4: First and second eigenmode of vocal fold vibration with the correspondent eigenfrequencies.

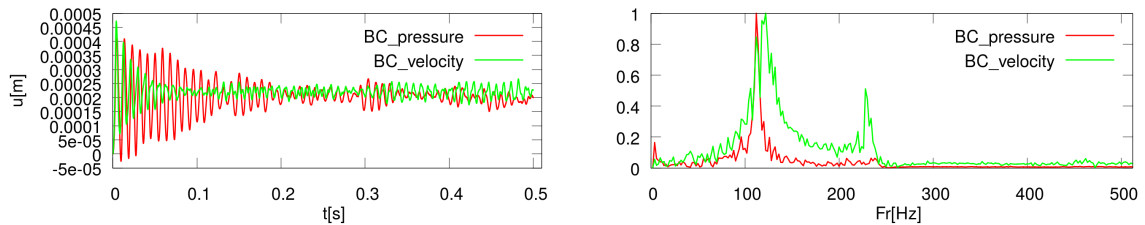


Figure 5: Simulated displacements of the point from the top of vocal fold in x -direction in time domain (left) and the normalized Fourier transformation of the signals (right). Time signal is plotted from the start of computation with the interaction.

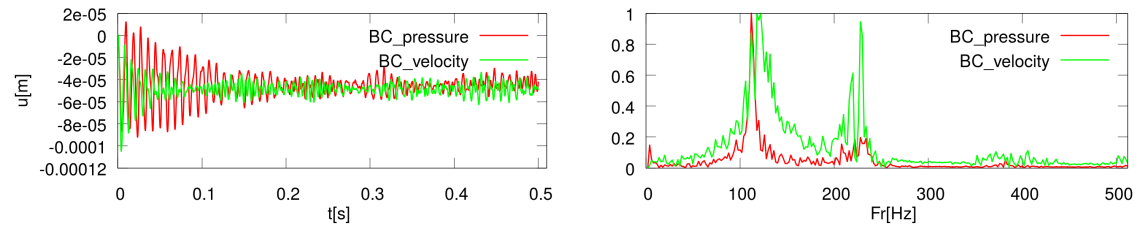


Figure 6: Simulated displacements of the point from the top of vocal fold in y -direction in time domain (left) and the normalized Fourier transformation of the signals (right). Time signal is plotted from the start of computation with the interaction.

eigenmode with the eigenfrequency of 108.7 Hz dominates in the spectrum for the x -component of the displacement (see Fig. 5). The frequency of the first eigenmode is also dominant for the y -component of the displacement but the second eigenmode with eigenfrequency 220.9 Hz is also excited noticeably (see Fig. 6). In the case of BC_velocity the excitation of the second mode is higher in comparison with the case of BC_pressure. This behaviour can be caused by different pressure distribution

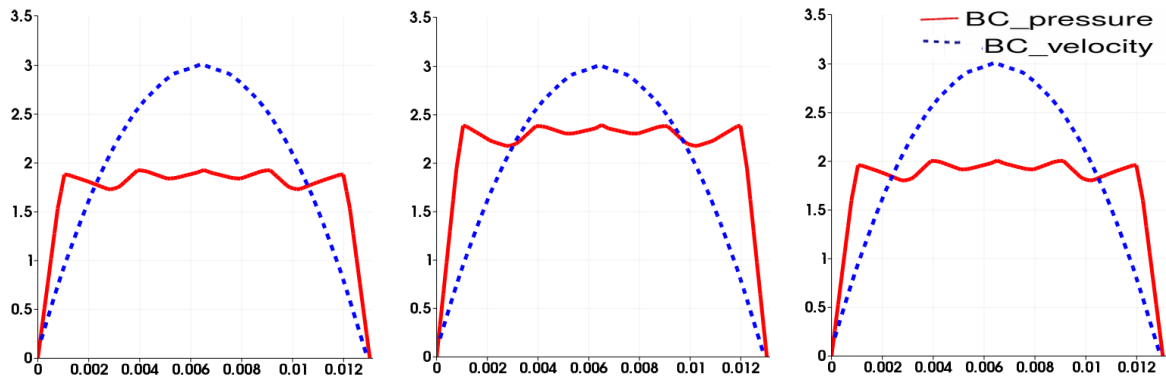


Figure 7: Velocity profile along the inlet at time instants $t = 0.1 + j * \Delta t$ [s], $j \in \{1, 4, 9\}$. Units are m/s and x -axis denotes distance from bottom of channel.

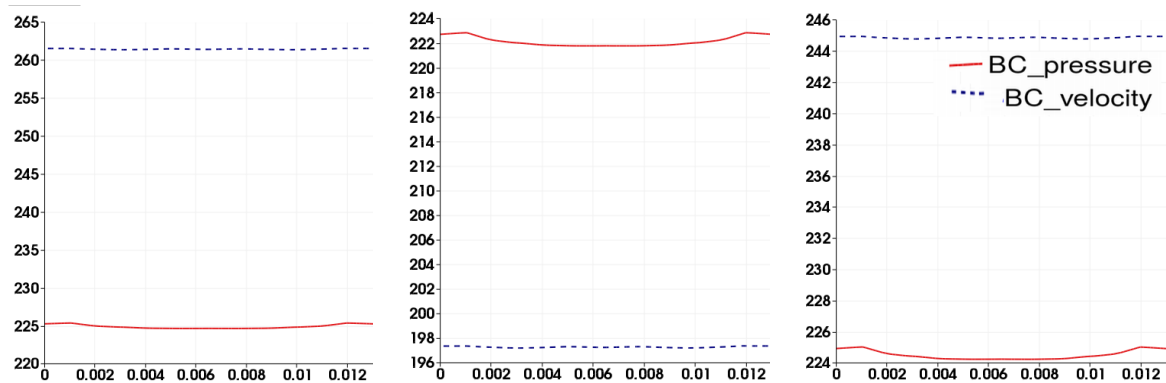


Figure 8: Kinematic pressure p along the inlet at time instants $t = 0.1 + j * \Delta t$ [s], $j \in \{1, 4, 9\}$. Units on the y -axis are in $\text{Pa} \cdot \text{m}^3/\text{kg}$ and the x -axis denotes the distance from the bottom of the channel.

inside the fluid domain which is the dominant part of the aerodynamic force. If the pressure difference is prescribed, then the real pressure drop between the inlet and the outlet remains almost constant while inlet velocity slightly varies. On the other hand if velocity profile is prescribed, then the inlet velocity is fixed and pressure along the channel considerably varies. This is presented in Figures 7 and 8, where time instants were chosen as: 1.0005 s – start of the vocal folds opening, 1.0020 s – point of return from maximal displacement, 1.0045 s – channel closure at the end of the vibration cycle.

5. Conclusion

The article presents the mathematical description and derivation of numerical scheme for solution of FSI by FEM. Special attention is paid to the stabilization of FEM by additional terms introduced in weak formulation of the problem. These

SUPG, PSPG and ‘div-div’ stabilization methods enable to overcome numerical instabilities and to obtain more accurate results. The simulation of flow-induced vibration of vocal folds computed by an in-house developed program is shown and the influence of the boundary conditions is studied.

Acknowledgements

This work was supported by grant No. GA16-01246S of the Czech Science Foundation and by grant No. SGS16/206/OHK2/3T/12 of CTU in Prague.

References

- [1] Braack, M. and Mucha, P. B.: Directional do-nothing condition for the Navier-Stokes equations. *J. Comput. Math.* **32** (2014), 507–521.
- [2] Brdička, M., Samek, L., and Sopko, B.: *Continuum mechanics*. Academia, 2000.
- [3] Clark, R. and Dowell, E. H.: *A modern course in aeroelasticity*. Springer, 2004.
- [4] Davis, T. A.: *Direct methods for sparse linear systems*. SIAM, 2006.
- [5] Feistauer, M., Sváček, P., and Horáček, J.: Numerical simulation of fluid-structure interaction problems with applications to flow in vocal folds. In: T. Bodnár, G.P. Galdi, and S. Nečasová (Eds.), *Fluid-structure Interaction and Biomedical Applications*, pp. 312–393. Birkhauser, 2014.
- [6] Gelhard, T., Lube, G., Olshanskii, M. A., and Starcke, J. H.: Stabilized finite element schemes with LBB-stable elements for incompressible flows. *J. Comput. Appl. Math.* **177** (2005), 243–267.
- [7] Richter, T.: *Numerical methods for fluid-structure interaction problems*. Ph.D. thesis, University of Heidelberg, Germany, 2010.
- [8] Scherer, R. C. et al.: Intraglottal pressure profiles for a symmetric and oblique glottis with a divergence angle of 10 degrees. *Journal of the Acoustical Society of America* **109** (2001), 1616–1630.
- [9] Takashi, N. and Hughes, T. J. R.: An arbitrary Lagrangian-Eulerian finite element method for interaction of fluid and a rigid body. *Comput. Methods Appl. Mech. Engrg.* **95** (1992), 115–138.
- [10] Valášek, J., Sváček, P., and Horáček, J.: On numerical approximation of fluid-structure interactions of air flow with a model of vocal folds. In: D. Šimurda and T. Bodnár (Eds.), *Topical problems of fluid mechanics 2016*, pp. 245–254. Institute of Thermomechanics, AS CR, v.v.i., 2015.